

Properties of entangled photon pairs generated by a CW laser with small coherence time: theory and experiment

Simone Cialdi*

INFN, Sezione di Milano, I-20133, Italy

Fabrizio Castelli†

*INFN, Sezione di Milano, I-20133, Italy and
Dipartimento di Fisica, Università di Milano, I-20113, Italy*

Matteo G. A. Paris‡

*Dipartimento di Fisica, Università di Milano, I-20113, Italy
CNISM, Udr Milano Università, I-20113 Milano, Italy and
ISI Foundation, I-10133 Torino, Italy*

The generation of entangled photon pairs by parametric down-conversion from solid state CW lasers with small coherence time is theoretically and experimentally analyzed. We consider a compact and low-cost setup based on a two-crystal scheme with Type-I phase matching. We study the effect of the pump coherence time over the entangled state visibility and over the violation of Bell's inequality, as a function of the crystals length. The full density matrix is reconstructed by quantum tomography. The proposed theoretical model is verified using a purification protocol based on a compensation crystal.

I. INTRODUCTION

Generation of entanglement is the key ingredient of quantum information processing. In optical implementation with discrete variables the standard source of entangled photon pairs is parametric down-conversion in nonlinear crystals pumped by single-mode laser [1]. Recent advances in laser diodes technology allow the realization of simpler and cheaper apparatuses for the entanglement generation [2, 3], though the quality of the resulting photon pairs is degraded by the small coherence time of the pump laser.

In this paper we address theoretically and experimentally the generation of entanglement using laser diode pump as well as its application to visibility and nonlocality tests. We focus on the effects of the small coherence time and implement a purification protocol based on a compensation crystal [4] to improve entanglement generation. We reconstruct the full density matrix by quantum tomography and analyze in details the properties of the generated state, including purity and visibility, as a function of the crystals length and the coherence time of the pump. The topic is relevant for applications for at least two reasons. On one hand quantifying the degree of entanglement is of interest in view of large scale application. On the other hand a detailed characterization of the generated state allows one to suitably tailor entanglement distillation protocols.

The paper is structured as follows: In Section II we

describe the experimental apparatus used to generate entanglement, whereas Section III is devoted to illustrate in details the quantum state of the resulting photon pairs in the ideal case. The effects of small coherence time are analyzed in Section IV and the experimental characterization of the generated states is reported in Section V. Section VI is devoted to nonlocality test whereas Section VII closes the paper with some concluding remarks.

II. THE EXPERIMENTAL APPARATUS

A scheme of the experimental apparatus is shown in Fig. 1. The “state generator” consists of two identical BBO crystals, each cut for Type-I down-conversion, one half-wave plate (HWP) and one quarter-wave plate (QWP) as implemented in [5]. The crystals are stacked back-to-back, with their axes oriented at 90° with respect to each other [1, 2]. The balancing and the phase of the entangled states are selected by changing the HWP and QWP orientation.

The crystals are pumped using a 40mW, 405-nm laser diode (Newport LQC405-40P), with a spectral line that is typically broadened by phonon collisions. The coherence time of the pump light τ_c , which is a fundamental parameter for our experiment, results 544 fs and correspond to a spectral width around 0.3 nm. We obtained this important information with a standard measurement of the first order correlation function. The generated photons are analyzed using adjustable QWP, HWP and a polarizer [6]. Finally light signals are focused into multimode fibers which are used to direct the photons to the detectors. The detectors are home-made single photon counting modules (SPCM), based on an avalanche photodiode operated in Geiger mode with active quenching. For the

*Electronic address: simone.cialdi@mi.infn.it

†Electronic address: fabrizio.castelli@mi.infn.it

‡Electronic address: matteo.paris@fisica.unimi.it

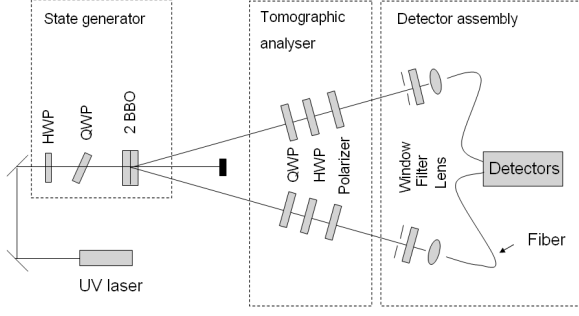


FIG. 1: Experimental apparatus for generating and analyzing entangled states.

coincidence counting we use a TAC/SCA.

The nonlinear crystals are properly cut to generate photons into a cone of half-opening angle 3.0° with respect to pump. The first crystal converts horizontally polarized pump photons into vertically polarized (V) signal and idler photons, while the second crystal converts vertically polarized pump photons into horizontally polarized (H) signal and idler photons. This configuration introduces a delay time $\Delta\tau$, depending on the crystal length, between the V and the H part of the entangled state, as discussed in the following Sections.

III. THE STATE VECTOR OF THE GENERATED ENTANGLED PHOTONS

The pair of photons generated by SPDC of Type I from a single nonlinear crystal, having wave vectors \vec{k}_s and \vec{k}_i , are represented by state vectors $|\vec{k}_s\rangle_s$ and $|\vec{k}_i\rangle_i$ for the signal and idler, respectively. The wavefunction appropriate to the system can be written as a superposition of these state vectors [7, 8, 9]:

$$|\Psi\rangle = \int d^3\vec{k}_s d^3\vec{k}_i A(\omega_p - \Omega_p^0) F(\Delta k_\perp) f(\Delta k_\parallel) |\vec{k}_s\rangle_s |\vec{k}_i\rangle_i \quad (1)$$

where $A(\omega_p - \Omega_p^0)$ is the spectral complex amplitude of the pump laser, which is a function of the pump frequency $\omega_p(k_p) = \omega_s(k_s) + \omega_i(k_i)$, assuming as usual the validity of the energy conservation in the generation process, and it is centered around the reference frequency Ω_p^0 . The factors F and f are mismatch functions depending on the variation of the transverse and longitudinal part of the pump wave vector with respect to the reference of momentum conservation, and are described in detail in the following.

The function $F(\Delta k_\perp)$ comes from a spatial integration over all the possible processes of photon generation within the pump transverse profile in the crystal, taking the first order approximation of the nonlinear interaction. For a Gaussian pump profile we obtain again a Gaussian function, with a width varying as the inverse of the beam

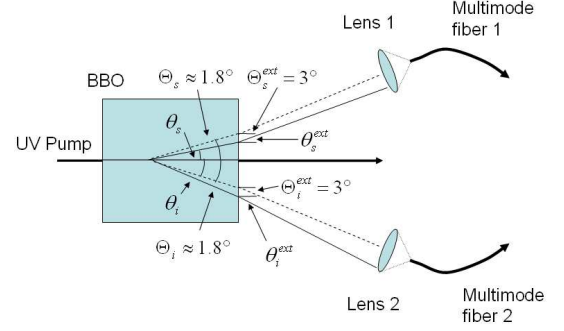


FIG. 2: Geometry for the generation of photon pairs.

waist w :

$$F(\Delta k_\perp) = e^{-w^2 \Delta k_\perp^2 / 4} \quad (2)$$

where, referring to Fig. 2, one has

$$\Delta k_\perp = k_s(\omega_s) \sin(\theta_s) - k_i(\omega_i) \sin(\theta_i)$$

with the internal generation angles θ_s and θ_i for signal and idler, respectively. In our case the pump beam waist is near 2 mm, therefore we can consider exact transverse momentum conservation to a good approximation. In fact it is easy to verify that with this beam waist we have an angular gaussian width of 0.006° around the reference internal angles $\Theta_s = \Theta_i = 1.8^\circ$ (derived from external angles $\Theta_s^{ext} = \Theta_i^{ext} = 3.0^\circ$ using Snell's law), very small with respect to the acceptance angle of 0.074° FWHM of the optical coupling devices. The conservation of the transverse wave vector permits to simplify the geometry of the system, by considering in the following a generation angle, say θ_i , as a function of the other quantities $\omega_s, \omega_i, \theta_s$.

The mismatch function $f(\Delta k_\parallel)$ has the same meaning of F , but derives from an integration along the crystal length L_C , and reads:

$$f(\Delta k_\parallel) = \frac{\sin(\Delta k_\parallel L_C / 2)}{\Delta k_\parallel L_C / 2} \quad (3)$$

where

$$\Delta k_\parallel = k_p(\omega_p) - k_s(\omega_s) \cos(\theta_s) - k_i(\omega_i) \cos[\theta_i(\omega_s, \omega_i, \theta_s)].$$

As a matter of fact the pump spectrum width, yet determining the visibility effects, is very small with respect to the spectral width of the down-conversion; this means that f is slightly dependent on $\omega_p = \omega_s + \omega_i$, as can be verified numerically. We will not consider such a dependence by substituting ω_p with the reference pump frequency Ω_p^0 as the argument of f . This approximation turns out to be very good for crystal lengths below a few mm, but around 3 mm (our maximum crystal length) the conservation of the longitudinal wave vector starts

to shrink the down-conversion spectrum. A similar consideration can be done over the dependence of f over the internal angle θ_s ; being the experimental configuration highly collinear, the optical couplers are practically insensible to its variation (within the acceptance cone). Therefore we can substitute θ_s with the fixed reference angle Θ_s , and the mismatch function becomes:

$$f(\omega_p, \omega_s, \theta_s) \approx f(\Omega_p^0, \omega_s, \Theta_s) \equiv f(\omega_s) \quad (4)$$

The wavefunction of the photon pair can now be written in the simpler form:

$$|\Psi\rangle = \int d\omega_p d\omega_s d\theta_s A(\omega_p - \Omega_p^0) f(\omega_s) \times |\omega_s, \theta_s\rangle_s |\omega_p - \omega_s, \theta_i(\omega_p, \omega_s, \theta_s)\rangle_i \quad (5)$$

In the first approximation we can solve for the integral over the internal generation angle θ_s because neither A nor f depend on it, but a more refined reasoning put forward the fact that the conservation of the transverse wave vector introduces a limitation in the effective spectral width of the mismatch function, hence affecting the integration over ω_s . This happens because by varying ω_s around the down-converted reference $\Omega_p^0/2$, the idler angle θ_i may go outside from the optical coupler acceptance limit, as verified by means of the experimental data discussed in Appendix A. This problem does not affect the integral over ω_p for the smallness of the pump spectral width. To take care of this spectral limitation we introduce a correction factor $R(\Omega_p^0/2, \Delta\omega_s)$ centered around the reference $\Omega_p^0/2$ and having the limited spectral width $\Delta\omega_s$ (see Appendix A). Defining $\tilde{f}(\omega_s) = f(\omega_s) \cdot R$, we arrive at this wavefunction for the photon pairs:

$$|\Psi\rangle = \int d\omega_p d\omega_s A(\omega_p - \Omega_p^0) \tilde{f}(\omega_s) |\omega_s\rangle_s |\omega_p - \omega_s\rangle_i \quad (6)$$

This expression is used to construct the proper wavefunction (or the proper state vector) for the entangled state generated in our experiment using the pair of oriented crystals [1, 2], as described in the previous Section. In particular we consider a suitable superposition of the

single crystal wavefunctions of eq. (6), introducing the degree of freedom of polarization on state vectors, because the first crystal generates a vertical polarized (VV) and the second crystal generates a horizontal polarized (HH) photon pairs, respectively. Moreover we have a delay time between these pairs, due to the different optical length of the photon trajectories in the inner of crystals. This can be represented in the model by assuming photon generation in the crystals middle [10, 11] (in Appendix B we show that this is a very good approximation) and introducing propagation factors for the internal state transport.

In the Fig. 3 a sketch of the geometry for entangled photon generation is shown, limited for clarity to the signal trajectories. In the first crystal V photons are generated, the state is $|V, \omega_s\rangle_s |V, \omega_p - \omega_s\rangle_i$, and the complex

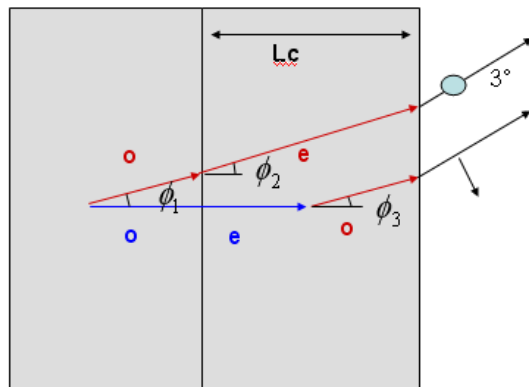


FIG. 3: Entangled photon generation and propagation inside the crystals. For clarity, only signal photon trajectories (red lines) are drawn (idler ones are symmetrically upset). The horizontal blue line is the pump ray. (o) and (e) indicates ordinary and extraordinary rays, respectively. L_c is the length of both crystals.

exponential for the product of the signal and idler propagation factor (as required by the form of eq. (6)) till to exiting the crystal is given by:

$$P(V) = \exp \left\{ iL_C \left[k_s^o(\omega_s) \frac{1}{2 \cos(\phi_1)} + k_i^o(\omega_p - \omega_s) \frac{1}{2 \cos(\phi_1)} + k_s^e(\omega_s) \frac{1}{\cos(\phi_2)} + k_i^e(\omega_p - \omega_s) \frac{1}{\cos(\phi_2)} \right] \right\} \quad (7)$$

where the superscripts (o) and (e) on wave vectors indicates ordinary and extraordinary propagation, and the angles $\phi_1 = 1.807$, $\phi_2 = 1.84$ can be found using the laws of wave rays in birefringent crystals [12] and Snell's law, under the request of an exit angle of 3° . For the second crystal, in which H photons are generated and the state is $|H, \omega_s\rangle_s |H, \omega_p - \omega_s\rangle_i$, the respective propagation factor is:

$$P(H) = \exp \left\{ iL_C \left[\frac{k_p^o(\omega_p)}{2} + \frac{k_p^e(\omega_p)}{2} + k_s^o(\omega_s) \frac{1}{2 \cos(\phi_3)} + k_i^o(\omega_p - \omega_s) \frac{1}{2 \cos(\phi_3)} \right] \right\} \quad (8)$$

where $\phi_3 = 1.806$, and it has been included the propagation of the pump ray from the generation point of the (VV) pair (note that ϕ_3 is slightly different from ϕ_2 due the different refraction index for o and e propagation). The

entangled state wavefunction is therefore:

$$|\Psi\rangle = \int d\omega_p d\omega_s A(\omega_p - \Omega_p^0) \tilde{f}(\omega_s) \frac{1}{\sqrt{2}} \{P(H) |H, \omega_s\rangle_s |H, \omega_p - \omega_s\rangle_i + P(V) |V, \omega_s\rangle_s |V, \omega_p - \omega_s\rangle_i\} \quad (9)$$

This expression can be recast in a more useful form in the following way. Let's write the frequencies as $\omega_p = \Omega_p^0 + \Omega_p$, $\omega_s = \Omega^0 + \Omega$ (with of course $\Omega_p^0 = 2\Omega^0$), where Ω_p and Ω represent the frequency shift with respect to reference for the pump and for the down conversion, respectively. Now, in the propagation factors we introduce a first order approximation for the wave vectors putting:

$$k_p(\omega_p) \approx k(\Omega_p^0) + \Omega_p/V_p, \quad k_s(\omega_s) \approx k(\Omega^0) + \Omega/V, \quad k_i(\omega_p - \omega_s) \approx k(\Omega^0) + \Omega_p/V - \Omega/V$$

where V_p and V are the proper group velocities of the pump and of the down converted signal, and these relations must be considered both for the ordinary wave and for the extraordinary wave. With these substitutions, and rewriting for future convenience the quantum states by factorizing the polarization part from the frequency one, the final form of the wavefunction eq. (9) read:

$$|\Psi\rangle = \int d\Omega_p d\Omega A(\Omega_p) \tilde{f}(\Omega^0 + \Omega) \frac{1}{\sqrt{2}} \cdot \left\{ e^{i(\phi_H + \tau_H \Omega_p)} |H\rangle_s |H\rangle_i |\Omega_p - \Omega\rangle_i + e^{i(\phi_V + \tau_V \Omega_p)} |V\rangle_s |V\rangle_i |\Omega_p - \Omega\rangle_i \right\} \quad (10)$$

where the phase terms coming from propagation factors are the sum of a constant phase:

$$\phi_H = \left\{ k^o(\Omega_p^0) + k^e(\Omega_p^0) + \frac{2k^o(\Omega^0)}{\cos(\phi_3)} \right\} \frac{L_C}{2},$$

$$\phi_V = \left\{ \frac{2k^o(\Omega^0)}{\cos(\phi_1)} + \frac{4k^e(\Omega^0)}{\cos(\phi_2)} \right\} \frac{L_C}{2}$$

and frequency dependent terms $\tau_H \Omega_p$, $\tau_V \Omega_p$ containing the total propagation time inside the crystals:

$$\tau_H = \left\{ \frac{1}{V_p^o} + \frac{1}{V_p^e} + \frac{1}{V^o \cos(\phi_3)} \right\} \frac{L_C}{2},$$

$$\tau_V = \left\{ \frac{1}{V^o \cos(\phi_1)} + \frac{2}{V^e \cos(\phi_2)} \right\} \frac{L_C}{2}$$

It is important to note that these delay factors depend on pump frequency (not on the down converted frequency); this fact can be interpreted saying that the states (HH) and (VV) exiting the crystals are generated from the pump in two different temporal events in the past, depending on the different trajectories across the crystals. For all these four phase factors, their numerical value are determined from the data on refraction indexes and group velocities taken from ref. [13], and listed in the following Table:

	pump		signal/idler	
	(o)	(e)	(o)	(e)
n	1.691719	1.659273	1.659984	1.632171
V	c/1.77878	c/1.73901	c/1.68376	c/1.65483

As a final observation, we note that in writing the final expression for the wavefunction eq. (10), it has been discarded the variation of the propagation factors with respect to the propagation angles. Due to small angular acceptance of the detectors, it is possible to verify that, with excellent approximation, this dependence does not introduce any relevant effect.

IV. THE POLARIZATION DENSITY MATRIX

For the calculation of the density matrix and the complete characterization of the wavefunction it is important to define at best the statistical properties of the CW pump radiation, because our experimental data depend strongly on its coherence length. In the temporal domain, this light is characterized by a (real) constant amplitude A_0 and a rapidly varying phase with a characteristic time equal to the coherence time of the pump τ_c . Therefore we can write:

$$\int d\omega A(\omega) e^{i\omega t} = A_0 e^{i\delta(t)} \quad (11)$$

where $\delta(t)$ is a proper fluctuating phase. The pump amplitude in the temporal domain can be considered as the Fourier transform of the complex spectral amplitude over a large time interval ΔT :

$$A(\omega) = \frac{1}{2\pi} \int_{\Delta T} dt A_0 e^{i\delta(t)} e^{-i\omega t} \quad (12)$$

Our experiment mainly concerns the reconstruction of the density matrix of the entangled system on the basis composed by the four signal and idler polarization combinations HH, HV, VH, VV . The relative density operator ρ , from which we derive the reduced density matrix on this polarization basis, is obtained from the full density operator $\rho_{\text{tot}} = |\Psi\rangle\langle\Psi|$ by tracing over frequencies, *e.g.* by integrating over the frequency state matrix elements:

$$\rho = \int d\omega'_p d\omega'_i \langle\omega'_p - \omega'_i|_s \langle\omega'|_s \langle\omega'|_s \langle\Psi|\Psi\rangle_s |\omega'_p - \omega'_i\rangle_i \quad (13)$$

corresponding to the fact that we do not perform frequency measurements.

The form of the wavefunction in eq. (10) implies that only four elements of the 4×4 reduced density matrix are different from zero. Using the general relation $\langle \omega | \omega' \rangle = \delta(\omega - \omega')$, we straightforwardly obtain for the first diagonal element:

$$\rho_{HH,HH} = \frac{1}{2} \int d\omega |f(\omega)|^2 \int d\omega_p |A(\omega_p)|^2 = \frac{1}{2} \epsilon A_0^2 \frac{\Delta T}{2\pi} \quad (14)$$

where we put $\epsilon = \int |f(\omega)|^2$ and $\int d\omega_p |A(\omega_p)|^2 = A_0^2 \Delta T / 2\pi$ from eq. (12). With similar calculation the other nonzero diagonal element results $\rho_{VV,VV} = \rho_{HH,HH}$, as expected by symmetry arguments.

For the two off diagonal elements one has $\rho_{HH,VV} = \rho_{VV,HH}^*$, and in particular:

$$\begin{aligned} \rho_{HH,VV} &= \frac{1}{2} \int d\omega |f(\omega)|^2 \int d\omega_p |A(\omega_p)|^2 e^{-i(\phi_H - \phi_V)} e^{-i\omega_p(\tau_H - \tau_V)} \\ &= \frac{1}{2} \epsilon e^{-i\phi} \int d\omega_p |A(\omega_p)|^2 e^{-i\omega_p(\tau_H - \tau_V)} \end{aligned} \quad (15)$$

where we put $\phi = \phi_H - \phi_V$. With the Wiener-Khinchine theorem this frequency integral can be recast as a two time correlation function over the interval ΔT , which can be taken very large with respect to the coherence time of the pump, and smaller than the detector response time:

$$\int d\omega_p |A(\omega_p)|^2 e^{-i\omega_p(\tau_H - \tau_V)} = A_0^2 \frac{\Delta T}{2\pi} \left(\frac{1}{\Delta T} \int_{\Delta T} dt e^{-i\delta(t) + i\delta(t - (\tau_H - \tau_V))} \right) = A_0^2 \frac{\Delta T}{2\pi} e^{-\Delta\tau/\tau_c} \quad (16)$$

where $\Delta\tau = |\tau_H - \tau_V|$, and the result is taken from Ref. [14]. If $\Delta\tau \gg \tau_c$ we have an incoherent superposition of random phases and the average of the complex exponentials tends to zero, otherwise we have a coherent sum, and the integral tends to one.

Finally, setting the state generator QWP in order to have $\phi = 0$ (see Ref. [1]) and putting for simplicity $p = e^{-\Delta\tau/\tau_c}$, the reduced density matrix is:

$$\begin{array}{cccc} & HH & HV & VH & VV \\ \begin{array}{l} HH \\ HV \\ VH \\ VV \end{array} & \left(\begin{array}{cccc} \frac{1}{2} & 0 & 0 & \frac{1}{2}p \\ 0 & 0 & 0 & 0 \\ 0 & 0 & 0 & 0 \\ \frac{1}{2}p & 0 & 0 & \frac{1}{2} \end{array} \right) & & (17) \end{array}$$

which can also be conveniently derived from a sum of two distinct density matrix, one of a pure entangled state and the other of a statistical mixture: $\rho = p \rho_e + (1-p)\rho_m$ where $\rho_e = |\Psi_e\rangle\langle\Psi_e|$ with $|\Psi_e\rangle = \frac{1}{\sqrt{2}}(|HH\rangle + |VV\rangle)$ and $\rho_m = \frac{1}{2}|HH\rangle\langle HH| + \frac{1}{2}|VV\rangle\langle VV|$. This is the more suitable form used for a comparison between theory and experimental data.

V. EXPERIMENTAL TOMOGRAPHIC RECONSTRUCTION OF THE DENSITY MATRIX AND CORRELATION VISIBILITY

In order to fully characterize the generated states at the quantum level we employ quantum tomography of their density matrices [15]. The experimental procedure goes as follows: upon measuring a set of independent two-qubit projectors $P_\mu = |\psi_\mu\rangle\langle\psi_\mu|$ ($\mu = 1, \dots, 16$) corresponding to different combinations of polarizers and phase-shifters, the density matrix may be reconstructed as $\rho = \sum_\mu p_\mu \Gamma_\mu$ where $p_\mu = \text{Tr}[\rho P_\mu]$ are the probabilities of getting a count when measuring P_μ and Γ_μ the corresponding dual basis, *i.e.* the set of operators satisfying $\text{Tr}[P_\mu \Gamma_\nu] = \delta_{\mu\nu}$ [16]. Of course in the experimental reconstruction the probabilities p_μ are substituted by their experimental samples *i.e.* the frequencies of counts obtained when measuring P_μ . In order to minimize the effects of fluctuations and avoid non physical results we use maximum-likelihood reconstruction of two-qubit states [6, 17]. At first we write the density matrix in the form

$$\hat{\rho} = \hat{T}^\dagger \hat{T}, \quad (18)$$

which automatically guarantees that $\hat{\rho}$ is positive and Hermitian. The remaining condition of unit trace $\text{Tr}\hat{\rho} = 1$ will be taken into account using the method of Lagrange multipliers. In order to achieve the minimal parametrization, we assume that \hat{T} is a complex lower tri-

angular matrix, with real elements on the diagonal. This form of \hat{T} is motivated by the Cholesky decomposition known in numerical analysis [18] for arbitrary non negative Hermitian matrix. For an M -dimensional Hilbert space, the number of real parameters in the matrix \hat{T} is $M + 2M(M - 1)/2 = M^2$, which equals the number of independent real parameters for a Hermitian matrix. This confirms that our parametrization is minimal, up to the unit trace condition.

In numerical calculations, it is convenient to replace the likelihood functional by its natural logarithm, which of course does not change the location of the maximum. Thus the function subjected to numerical maximization is given by

$$L(\hat{T}) = \sum_{k=1}^N \ln \text{Tr}(\hat{T}^\dagger \hat{T} P_{\mu_k}) - \lambda \text{Tr}(\hat{T}^\dagger \hat{T}), \quad (19)$$

where λ is a Lagrange multiplier accounting for normalization of $\hat{\rho}$ that equals the total number of measurements N . This may be easily proved upon writing $\hat{\rho}$ in terms of its eigenvectors $|\phi_\mu\rangle$ as $\hat{\rho} = \sum_\mu y_\mu^2 |\phi_\mu\rangle \langle \phi_\mu|$, with real y_μ , the maximum likelihood condition $\partial L / \partial y_\nu = 0$ reads

$$\lambda y_\nu = \sum_{k=1}^N \frac{y_\nu \langle \phi_\nu | P_{\mu_k} | \phi_\nu \rangle}{\text{Tr}(\hat{\rho} P_{\mu_k})}, \quad (20)$$

which, after multiplication by y_ν and summation over ν , yields $\lambda = N$.

The above formulation of the maximization problem allows one to apply standard numerical procedures for searching the maximum over the M^2 real parameters of the matrix \hat{T} . The examples presented below use the downhill simplex or the simulated annealing methods [19]. Results of the reconstruction are reported for crystals with three different thicknesses, precisely 0.5, 1 e 3 mm, and in the case of compensation of the delay time between generated photons, as discussed later. Moreover we present an analysis on the direct measurement of the visibility of the entangled state.

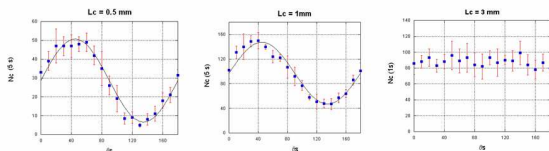


FIG. 4: Entangled state visibility as a function of the polarizer angle, for generating crystals of 0.5, 1 e 3 mm thickness.

Data on correlation visibility are simply obtained by removing the HWP and QWP plates of the tomographic analyzer (see Fig. 1) and detecting the signal and idler coincidence counts in a time interval, as a function of the signal polarizer angle, and having fixed the idler polar-

ization angle at 45° . The theoretical prediction is:

$$P(\xi_s, 45_i^\circ) = {}_i \langle 45^\circ | {}_s \langle \xi_s | \rho | \xi_s \rangle_s | 45^\circ \rangle_i \\ = \frac{1}{2} p (\cos(\xi_s - 45^\circ))^2 + \frac{1}{4} (1 - p) \quad (21)$$

where ξ_s is the angle of the signal polarizer in the counter-clockwise direction, with the horizontal axis as the 0° reference. As it is apparent from this formula, when p is near the unity (delay time smaller with respect the coherence time of the pump) the oscillating contribute due to the non-local correlations is dominant. On the contrary, with greater delay time (and small p) the correlations are washed out and the result is that of a statistical mixture which does not depend on the angle. In particular, the maximum of $P(\xi_s, 45_i^\circ)$ is at 45° , while the minimum is at 135° , hence we can write explicitly the visibility \mathcal{V} of the oscillation as:

$$\mathcal{V} = \frac{P(45_s^\circ, 45_i^\circ) - P(135_s^\circ, 45_i^\circ)}{P(45_s^\circ, 45_i^\circ) + P(135_s^\circ, 45_i^\circ)} = p \quad (22)$$

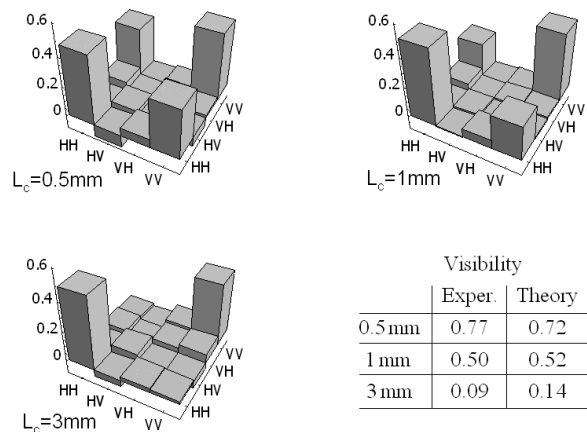


FIG. 5: Tomographic reconstruction of the generated state for three different crystals. The measured and calculated visibility are shown in table.

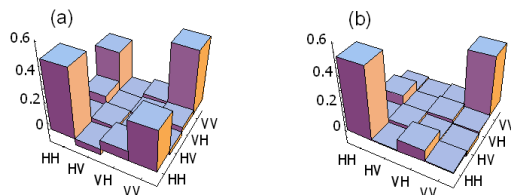


FIG. 6: Tomographic reconstruction with a delay compensation crystal (see text). (a) Crystal angle set for maximum compensation, visibility 0.66. (b) Crystal angle at 90° with respect to (a), visibility 0.17.

In Fig. 4 we show the visibility measurements as a function of the signal polarizer angle for the three different crystal pairs, with the theoretical prediction of eq. (22) indicated by a full line. The comparison between the theoretical density matrix elements of eq. (17) and their tomographic reconstruction from experimental data is shown in Fig. 5. It is confirmed that the off diagonal elements tend to reduce in magnitude for larger crystal thickness; in particular for 3 mm crystals we obtain the density matrix of a statistical mixture.

In our model the lack of visibility of the entangled state is fully ascribed to the decoherence effect due to the fluctuating phase difference between H and V parts of the SPDC, depending on the delay $\Delta\tau$. Having a very small area of the fiber collimator, we have neglected any decoherence of spatial origin, which introduces a phase variation depending on the detector viewing angle. In order to verify this statement, we have performed a series of measurements with the 3 mm crystal, putting windows of 0.5 mm linear aperture in front of the collimators: if the decoherence had a spatial contribution, we would have expected an increasing in the state purity. In fact, the results of the state reconstruction were the same as the original configuration, thus supporting our hypothesis.

This fact also suggests how to improve the purity of the entangled state by a phase retardation on the H polarized part of the pump with respect to the V polarized part, to get $\delta_H(t + \Delta\tau) = \delta_V(t)$. This can be approximately accomplished by inserting, along the pump ray and before the state generator, a properly oriented BBO crystal with a suitable length. We performed a series of measurements using the 1 mm double crystal as state generator, and a 3 mm single crystal as pump phase retarder. By varying the orientation of the axis of this crystal, we have compensation or enhancement of the effect of the time delay between the parts of the generated entangled state. In particular, the visibility is expected to vary from a maximum to a minimum for a 90° change in orientation, as confirmed by the tomographic reconstruction shown in Fig. 6. Notice that the maximum visibility of 0.66 is larger than the corresponding visibility without the auxiliary crystal (see Fig. 5), thus demonstrating a partial time delay compensation.

VI. MEASUREMENTS ON THE VIOLATION OF BELL'S INEQUALITY

We have also performed a series of measurements of the S parameter, characterizing the Bell's inequality in the CHSH version [20], for a comparison with the prediction of our theoretical model. To obtain reliable data on the S parameter we used the same experimental apparatus previously employed for correlation measurements. We considered as usual the 16 different configuration of the polarization angles on the signal and on the idler [2].

The Bell S parameter is theoretically defined as:

$$S = E(a, b) - E(a, b') + E(a', b) + E(a', b') \quad (23)$$

where the arguments a, a' and b, b' are the selected angles for signal polarizer and idler polarizer, respectively. The function E is defined as $E(\alpha, \beta) = P(\alpha, \beta) + P(\alpha^\perp, \beta^\perp) - P(\alpha, \beta^\perp) - P(\alpha^\perp, \beta)$, where $\alpha^\perp = \alpha + 90^\circ$ e $\beta^\perp = \beta + 90^\circ$. The function P is exactly that described in eq. 21, but with the idler angle specified by the argument. For any realistic local theory one has $|S| \leq 2$, while for quantum mechanics $|S|$ can be greater than 2, reaching a maximum value of $2\sqrt{2}$. The following choice for the angles is used: $a = 0^\circ$, $b = \theta$, $a' = b + \theta$ and $b' = a' + \theta$. In this way S is a function of the angle θ alone. In Fig. 7 we show the calculated $S(\theta)$ for three states with different visibility $\mathcal{V} = p = (1, 0.7, 0.5)$; by decreasing p , the values of S tend to return in the limit of a local theory.

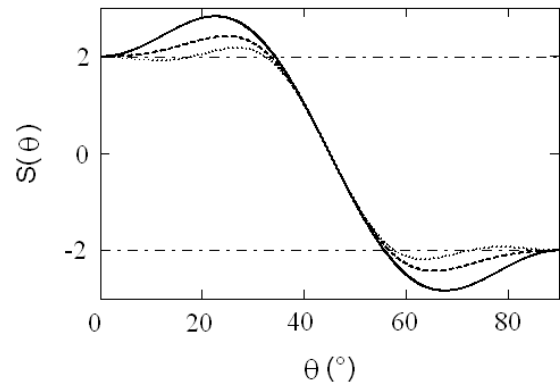


FIG. 7: S parameter as a function of θ for three different visibility values. Full line: $\mathcal{V} = 1$; dashed line; $\mathcal{V} = 0.7$; dotted line $\mathcal{V} = 0.5$.

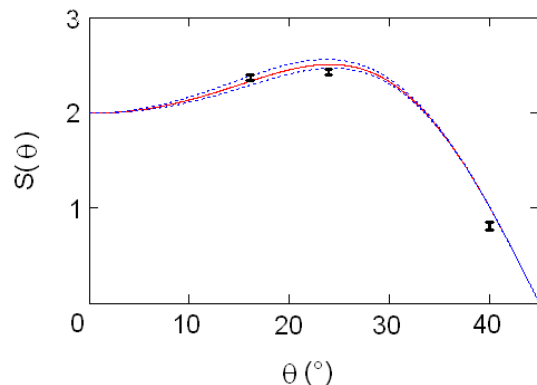


FIG. 8: Experimental results for S parameter for three values of θ , compared with the theoretical S for a visibility of 0.77.

For a comparison with these results of our model, we have measured the S parameter for three different angles using as state generator the pair of 0.5 mm crystals, that is the case with higher visibility. In Fig. 8 we show the theoretical curve of the S parameter for a visibility equal to 0.77 (full line), together with two other curves (dashed lines) indicating the extremal of the experimental errors,

relative to the limited number of count during data acquisition. The three measurements of S for the angles of 16° , 24° , 40° are indicated with error bars. In particular we get $S(16^\circ) = 2.38 \pm 0.03$, $S(24^\circ) = 2.417 \pm 0.025$ and $S(40^\circ) = 0.80 \pm 0.05$. From these data we can conclude that in the case of 24° the Bell's inequality is violated for more than 17 standard deviations.

VII. CONCLUSIONS

We have analyzed, both theoretically and experimentally, the generation of polarization-entangled photon pairs by parametric down-conversion from solid state CW lasers with small coherence time. In particular, we have analyzed in some details a compact and low-cost setup based on a two-crystal scheme with Type-I phase matching. The effect of pump coherence time on the entanglement and the nonlocality has been studied as a function of the crystals length. The full density matrix has been reconstructed by quantum tomography and the proposed theoretical model is verified using a purification protocol based on a compensation crystal. We conclude that laser diodes technology is of interest in view of large scale application and that its that the characterization of the generated state allows one to suitably tailor entanglement distillation protocols.

Acknowledgements

MGAP thanks Maria Bondani e Marco Genovese for useful discussions. We are also indebted with Stefano La Torre for his help in detector realization.

APPENDIX A: MEASUREMENT OF THE COHERENCE LENGTH

In this Appendix we experimentally verify that the spectrum of the down-converted signal is reduced when coincidence photon counts are performed, as a consequence of the trasverse momentum conservation.

If we observe only a single photon of the generated pair, the part of the spectrum incident on the coupling device is described in practice by the mismatch function $f(\omega_s)$ defined in Eqs. (3) and (4). But if we observe both photons and measure the simultaneous counts between signal and idler, we will detect a spectrum with a smaller width, and therefore we have a greater coherence length of the radiation. This because if we have a very wide spectrum for the signal at a fixed angle of observation, the idler photons, correlated with the signal photons also by transverse momentum conservation, will be dispersed over an angle that can be wider with respect to the acceptance angle of the coupling device. Hence the pair of coupling devices work as a filters limiting the spectral

window for observation. To the purpose of a determination of this effective spectral width, we present here some measurements using interference methods. In particular we performed two series of measurements, the first relative to the direct counts on a single detector to find the width associated with $f(\omega_s)$, the second relative to the coincidence counts on the two detectors to determine the width of the corrected mismatch function $\tilde{f}(\omega_s)$ used in eq. (6).

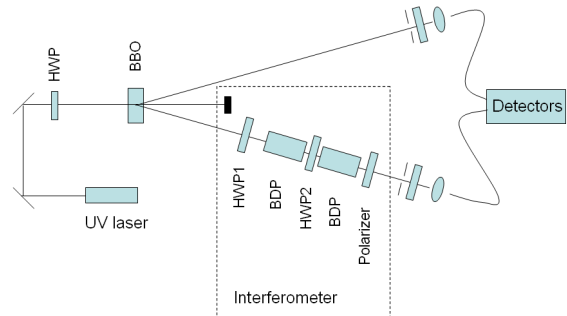


FIG. 9: Sketch of the experimental apparatus for the measure of the coherence length.

In Fig. 9 we show the experimental scheme (based on a single BBO crystal) employed for these types of measurements. An interferometer equal to that described in [5] is placed among the signal ray. This interferometer is easy to align and is a very stable device. In both types of counting measurements we expect to see interference fringes as a function of the delay time introduced by the interferometer between two optical paths, and within the radiation coherence time. In particular we would determine a greater coherence length in the case of coincidence counts with respect to the case of signal single counts.

The theoretical description of the interferometric experiment is as follows. In the case of a single photon observation, and with a crystal generating horizontal photons, the density matrix for the signal before the interferometer can be built with the wavefunction of eq. (10) of Section III by neglecting vertical polarization states, and tracing over the idler frequency:

$$\rho_1 = \int d\Omega |f(\Omega^0 + \Omega)|^2 |H, \Omega\rangle_s \langle H, \Omega| \quad (\text{A1})$$

where we do not consider the immaterial propagation factor and use the original mismatch function of eq. (4).

The density matrix after the interferometer follows by considering: (a) a polarization rotation of 45° due to the HWP plate placed before the first calcite crystal; (b) the delay time τ introduced by the interferometer between the H and V parts; (c) the projection of these states over the axis of the final polarizer oriented at 45° , placed before the coupling device. The final density matrix is easily obtained as:

$$\rho_1 = \int d\Omega |f(\Omega^0 + \Omega)|^2 \frac{1}{4} |1 + e^{i\Omega\tau}|^2 |45^\circ, \Omega\rangle_s \langle 45^\circ, \Omega| \quad (\text{A2})$$

The probability to observe a count on the detector is then proportional to:

$$\begin{aligned} P_1(\tau) i &= \int d\Omega' {}_s\langle 45^\circ, \Omega' | \rho_1 | 45^\circ, \Omega' \rangle_s \\ &= \int d\Omega |f(\Omega^0 + \Omega)|^2 \frac{1}{4} |1 + e^{i\Omega\tau}|^2 \quad (\text{A3}) \end{aligned}$$

The width of the interference pattern representing count numbers as a function of the delay τ , is given by a factor similar to a Fourier transform of the down-converted power spectrum; hence this width scales as the inverse of the spectral power width of the function f .

In the case of signal and idler coincidence counting, the state vector is again derived from eq. (10), by taking only the H part and discarding the propagation factor. After the passage in the interferometer, it is straightforward to see that the coincidence probability is the same as for the single count probability by replacing $f(\Omega^0 + \Omega)$ with the modified mismatch function $\tilde{f}(\Omega^0 + \Omega)$. Hence in this case the width of the interference curve is governed by the modified spectral power width $\Delta\omega_s$ of \tilde{f} .

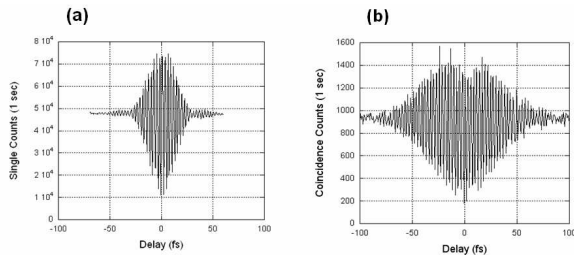


FIG. 10: Interference patterns: (left) single signal counts; (right) signal and idler coincidence counts.

In Fig. 10 we show on the left the interference pattern obtained with signal single counts, using the BBO crystal of 3 mm length. The width of the curve is near 30 fs, corresponding to a down converted spectrum of about 64 nm. On the right we show the pattern in the case of signal and idler coincidence counts: the coherence time is enlarged to 70 fs, corresponding to a spectral width of 27 nm. In both cases the coherence length is well below that of the pump light. These data are used to determine the appropriate correction factor $R(\Delta\omega_s) = \tilde{f}(\omega_s)/f(\omega_s)$ in the definition of the wavefunction eq. (6).

APPENDIX B: COMPLETE CALCULATION OF THE DELAY TIMES IN STATE GENERATION

In deriving the delay time between (HH) and (VV) photons, we assumed state generation in the crystals mid-

dle. But in fact these states can be generated in any point in the inner of the crystals, therefore the propagation factors $P(H)$ and $P(V)$ must be position dependent. Let's indicate with z_1 and z_2 the longitudinal coordinates of the internal generation points for the first crystal and for the second crystal, respectively. Referring to the Fig. 3, we now have the following two equations for the propagation times τ_H and τ_V :

$$\tau_H(z_1, z_2) = \frac{L_C - z_1}{V_p^o} + \frac{z_2}{V_p^e} + \frac{L_C - z_2}{V^o \cos(\phi_3)} \quad (\text{B1})$$

$$\tau_V(z_1, z_2) = \frac{L_C - z_1}{V^o \cos(\phi_1)} + \frac{L_C}{V^e \cos(\phi_2)} \quad (\text{B2})$$

Generally speaking, the state visibility p would depend on the delay time $\Delta\tau(z_1, z_2) = \tau_H(z_1, z_2) - \tau_V(z_1, z_2)$. Because we do not have any information about the effective position in which a particular photon pair is generated, we consider an average over the possible positions, by integrating with a flat distribution probability:

$$p_z = \frac{1}{L_C^2} \int dz_1 dz_2 e^{-\Delta\tau(z_1, z_2)/\tau_c} \quad (\text{B3})$$

In Fig. 11 we show a comparison between the visibility for state generation in the crystals middle, and that obtained from the above formula. It is clear that there is some difference only for very small visibilities obtained with very long crystals.

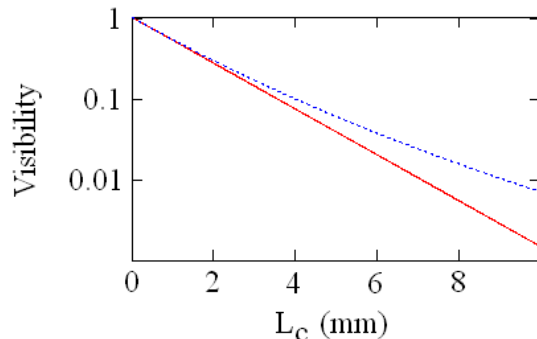


FIG. 11: Entangled state visibility as a function of the crystal length for the different assumptions on the state generation position. Full line: in the crystals middle; Dotted line: in the whole crystal length.

-
- [1] P.G. Kwiat, E. Waks, A.G. White, I. Appelbaum, and P.G. Eberhard, Phys. Rev. A **60**, R773 (1999).
- [2] D. Dehlinger and M.W. Mitchell, Am. J. Phys. **70**, 903 (2002).
- [3] S. Cialdi, F. Castelli, I. Boscolo, M.G.A. Paris, Appl. Opt., in press.
- [4] Y. Nambu, K. Usami, Y. Tsuda, K. Matsumoto, K. Nakamura, Phys. Rev. A **66**, 033816 (2002).
- [5] A. Gogo, W.D. Snyder, and M. Beck, Phys. Rev. A **71**, 052103 (2005).
- [6] D.F.V. James, P.G. Kwiat, W.J. Munro, and A.G. White, Phys. Rev. A **64**, 052312 (2001).
- [7] C. K. Hong, L. Mandel, Phys. Rev. A, **31** 2409 (1985)
- [8] A. Joobeur, B. E. A. Saleh, M. C. Teich, Phys. Rev. A **50**, 3349 (1994)
- [9] A. Joobeur, B. E. A. Saleh, T. S. Larchuk, M. C. Teich, Phys. Rev. A **57**, 4360 (1996).
- [10] G. Brida, M. Chekhova, M. Genovese, L. Krivitsky, Phys. Rev. A **76**, 053807 (2007).
- [11] G. Brida, M. V. Chekhova, M. Genovese, L. A. Krivitsky, Opt. Exp. **15**, 10182 (2007).
- [12] Yariv and Yeh, "Optical waves in crystals" (John Wiley and Sons INc., Hoboken, New Jersey, 2003).
- [13] A.V. Smith, SNLO nonlinear optics software, SANDIA National Labs. (<http://www.sandia.gov/imrl/X1118/xxtal.htm>)
- [14] K. Blushs and M. Auzinsh, Phys. Rev. A **69**, 063806 (2004).
- [15] M.G.A. Paris and J. Rehacek (Eds), "Quantum state estimation", Lect. Not. Phys. **649** (2004).
- [16] G.M. D'Ariano, L. Maccone, and M.G.A. Paris, Journ. of Phys. A, **34**, 93 (2001).
- [17] K. Banaszek, G.M. D'Ariano, M.G.A. Paris, and M.F. Sacchi, Phys. Rev. A **61** 10304 (2000).
- [18] A. S. Householder: *The Theory of Matrices in Numerical Analysis* (Blaisdell, New York, 1964) Sec. 5.2
- [19] W. H. Press, S. A. Teukolsky, W. T. Vetterling, B. P. Flannery: *Numerical Recipes in Fortran: The Art of Scientific Computing* (Cambridge University Press, Cambridge, 1992) Sec. 10.4
- [20] J. F. Clauser, M. A. Horne, A. Shimony, R. A. Holt, Phys. Rev. Lett. **23** (15), 880-824 (1969)